Express Polymer Letters Vol.16, No.4 (2022) 388–409
Available online at www.expresspolymlett.com
https://doi.org/10.3144/expresspolymlett.2022.29

Research article

Impact of corona and radio-frequency plasma treatment on the degradation of poly(3-hydroxybutyrate-*co*-3-hydroxyvalerate) (PHBV)

Ana Antunes, Anton Popelka, Adriaan Stephanus Luyt, Abdelrahman Mahmoud, Omar Yosef Aljarod, Mohamed Hassan, Peter Kasak*

Center for Advanced Materials, Qatar University, PO Box 2713, Doha, Qatar

Received 9 August 2021; accepted in revised form 17 November 2021

Abstract. Poly(3-hydroxybutyrate-*co*-3-hydroxyvalerate) (PHBV) is a polyester, produced naturally by microorganisms, with excellent biocompatibility. Corona and radio-frequency (RF) plasma treatment were applied in order to improve the degradation process of PHBV. Samples were subjected to an accelerated weathering test for 500, 1000, and 2000 h of weathering exposure and to natural weathering for one year. Various analytical, spectroscopic, and microscopic techniques have been used to analyze the degradation process. This study revealed that corona and RF plasma treatment acted as a hydrolytic and ultraviolet light (UV) degradation promoter for PHBV. Both plasma treatments chemically modify the PHBV surface resulting in better wettability contributing to the hydrolytic degradation. Microscopic analysis revealed a rougher defects-containing surface of plasma-treated PHBV in comparison with untreated PHBV after the degradation process, promoting deeper water diffusion and UV penetration. The photo- and hydrolytic degradation caused significant surface changes of plasma-treated PHBV after 2000 h of accelerated weathering and one year of natural weathering. Moreover, deterioration in mechanical properties has been more pronounced in the RF plasma-treated samples. These results demonstrate the potential use of plasma treatment on improving the degradability of PHBV.

Keywords: *biodegradable polymers, plasma treatment, accelerated degradation, natural weathering, mechanical properties*

1. Introduction

Poly(3-hydroxybutyrate-*co*-3-hydroxyvalerate), which is commonly known as PHBV from the polyhydroxyalkanoate polymer family, is an aliphatic thermoplastic polyester naturally produced by bacteria with excellent biocompatibility and biodegradability. In general, PHBV is used in packaging and controlled release of drugs, as well as in medical and engineered devices [1–4]. The PHBV structure consists of two parts, *i.e.*, the poly(3-hydroxybutyrate) (PHB) and the 3-hydroxyvalerate (HV) fractions. The properties of the copolymer greatly depend on the comonomer ratio distribution. For instance, if the content of the side group HV is greatly increased, the brittle characteristics of PHB are changed, which increases its toughness and decreases crystallinity, glass transition, melting temperature, and crystallization rate. PHBV is a polymer with low crystallinity and high flexibility, which eases its ability to be processed. Furthermore, HV and associated physical properties are responsible for biodegradability as it increases with the HV content [5–7].

Most of the degradation studies on PHBV have focused on its biodegradation behavior when exposed to water [1, 4, 8], soil [7, 9–11], waste compost [12, 13], and enzymes [14–16]. PHBV exposed to weathering significantly decreases in molar mass due to chain scission, and it was defined by the hydroxybutyrate-

*Corresponding author, e-mail: anton.popelka@qu.edu.qa

ydroxyvalerate units [17]. The main property that showed a significant increase was the crystallinity for PHBV, which was increased by 20% after being exposed to weathering conditions [18]. Different tests like tensile tests showed that after conditioning the PHBV by weathering the ultimate strength and elongation at break were the two main features. Based on experimental findings for PHBV, radical initiation, Norrish I/II, and hydrolysis degradation mechanisms were proposed as degradation mechanisms [19].

Several approaches for the acceleration of degradation of the bio-based polymer have been introduced, such as blending with other components, compounding, and surface modification [20, 21]. Blending and compounding require the involvement of another component that changes material formulation. More industrially feasible is a physical modification of a bio-based polymer surface, such as plasma treatment, since this approach represents an eco-friendly, dry, solvent-free, low-cost process [22–26]. Physical bombardment of polymer surface by plasma excited species results in crosslinking, grafting, etching, roughening, and functionalization. This method is used mainly to increase the surface free energy of the material and improve its adhesive properties and biocompatibility [27]. Apart from such utilization, plasma treatment is responsible for degradation processes due to the interaction between the plasma-created species and the polymer surface, which causes etching and thus forms new radical and functional groups. Low-temperature plasma treatment of biodegradable polymers can positively affect their biodegradability by a wettability improvement through the incorporation of polar functional groups, such as hydroxyl, carbonyl, and carboxyl groups [28]. Fabbri *et al*. [29] studied an effect of plasma treatment on poly(butylene succinate)-based copolymer. The improved wettability resulted in an increased hydrolytic degradation rate. The surface treatment by plasma is considered as an effective approach to increase wettability, which can promote the moisture attack during a degradation process under weathering conditions. The results indicated that physical modification of the surface, such as roughness, and the new functional groups such as –OH, COO– and –CO– that improved the wettability of the treated surfaces, absorbing more water than untreated PHBV, and the degree of absorption depends on the applied plasma discharge power [30, 31]. Kim and Masuoka [32] confirmed the increased chemical degradability of PHBV treated with CO_2-plasma in both acid and base environments, which was the result of increased roughness and wettability. Many parameters guide the successful application of the plasma treatment, such as substrate properties, exposure time, gas types and pressure, temperature, and plasma type, such as corona or radio-frequency (RF) [4]. Compared with conventional wet modification methods, plasma treatment has many advantages, such as being environmentally friendly, producing no waste, being non-hazardous, and being a fast and dry process [33]. Therefore, it is demanded to investigate the influence of the different types of initial plasma treatment for the subsequent degradation of PHBV as a promising polymeric material. That allows a deeper understanding of the degradation process for tailoring utilization and permits controlled and tunable degradation.

In this work, air corona and RF plasma treatment were used to modify the PHBV surface for improving its degradability utilizing the photo-aging effect applicable in packaging applications. Preliminary studies were done for the optimization of the exposure time. The aim was to study the effects of both plasma treatments on the properties of the PHBV after accelerated weathering degradation, which was compared with natural weathering.

2. Experimental

2.1. Materials

The PHBV containing 25% of 3-hydroxyvalerate segments in the polymer was obtained from Pensieve Technology Co., Ltd. (Wuhan, China). It is light yellow with a density of 1.24 g·cm^{-3}, a melt flow index of 3.2 g/10 min at 190 °C, glass transition around –45 °C, and a melting temperature of ~90 °C. The molar mass dispersity of neat PHBV is 1.41, showing 59 228 and 83 362 g·mol^{-1}, for M_n and M_w, respectively.

Ethylene glycol (>98% FLUKA, Morris Plains, New Jersey, USA), formamide (>98% FLUKA Morris Plains, New Jersey, USA) and ultra-pure water (prepared by Purification System Direct Q3, Millipore Corporation, Molsheim, France) were used as testing liquids for wettability analyses.

2.2.Preparation method

The polymer was first dried in an oven at 50 °C overnight before a sample preparation. The neat PHBV was then placed between two pieces of stainless steel plate covered by a release foil and molded

into 1 mm thick sheets at 120 °C for 10 min using a hydraulic press (Carver, Inc., Wabash, Indiana, USA) at a pressure of 50 bar. The sheets were allowed to cool at room temperature and then cut into dumbbell and rectangular shapes as further described.

2.3. Plasma treatment

Corona system CVE-L (Softal, Hamburg, Germany) working at atmospheric pressure was used for the surface treatment of the PHBV samples under dynamic conditions. This system generates corona discharge in an air atmosphere using generator 7010 (Softal, Hamburg, Germany) with a maximum 300 W of nominal corona power and 20.8 kHz frequency at 8.4 A of output current. The corona system consists of a set of powered ceramic electrodes for a maximum of 29.70×1.35 cm^2 treated area embedded in a ceramic insulator for the optimal isolation of high voltage. A planar sample holder made of porous aluminum with suction control keeps the samples in the right position during the treatment. A high-efficiency catalytic ozone removal system is part of this system for efficient ozone extraction, ensuring a safe working environment. The plasma treatment process of the PHBV samples was optimized in terms of treatment times varied from 1 to 12 s using 300 W of nominal power, and 1 mm was the distance between electrodes and samples holder.

A Venus75-HF plasma system (PlasmaEtch, Carson, CA, USA) working under vacuum and 13.56 MHz RF was used for the surface treatment of the PHBV samples under static conditions. This equipment consists of a cylindrical chamber made of aluminum (25 cm in diameter and 28 cm in deep). A capacitive parallel plate design allows generating nominal power with a maximum of 120 W. All the operational parameters are fully controllable by the PC software, such as treatment time or nominal power, for achieving an optimal plasma treatment process of the samples. The RF plasma treatment of the PHBV samples was first optimized in terms of various treatment times (15–180 s).

2.4. Accelerated weathering aging

The accelerated weathering of the plasma-treated samples, *i.e.*, untreated, corona treated PHBV, and RF treated PHBV samples, were conducted in an accelerated weathering tester Model QUV/se (Q-LAB, Westlake, Ohio, USA). The weathering conditions were following the Cycle-C of the ASTM D4329 standard. Fluorescent UV lamps (UVA-340, Q-LAB, Westlake, Ohio, USA) with 0.76 $W \cdot m^{-2}$ irradiance (wavelength 340 nm) were used with cycles of 8 h UV irradiation at 50 °C, followed by four h dark at 50 °C under 100% condensing humidity. These consecutive cycles were applied to the specimens attached to the test panels without any interruption. The effects of the accelerated weathering were investigated for four exposure periods: 0, 500, 1000, and 2000 h. Samples were collected for analysis after each period, and they were designated as 'PHBV/xh', 'PHBV/Corona/xh' or 'PHBV/RF/xh', respectively for corona and RF treatment, where x denotes the accelerated weathering period in hours.

2.5. Natural weathering aging

The natural weathering (NW) exposure of PHBV and plasma-treated PHBV samples were carried out in the Middle East region, in Doha (Qatar, GPS coordinates 25.257071, 51.423344) for one year, from August 2019 to August 2020. A total of 12 daily hours of sun exposure were observed. Over this period of time, the highest reported values for temperature and humidity were 50 °C and 82%, respectively, and the lowest values were 23 °C and 24%. The samples were suspended with grips on a pole. The exposed samples were only removed for characterization at the end of this period.

2.6. Wettability analysis

The video-based optical contact angle measuring system OCA35 (DataPhysics, Filderstadt, Germany) was used to measure surface wettability changes of the PHBV samples after plasma treatment and the aging effect. Sessile drop measurements were carried out. Testing liquids with different surface tensions, such as ultra-pure water, formamide, ethylene glycol, were used to evaluate the surface free energy of the untreated and treated samples for the analysis of wettability changes after corona treatment and the aging effect. A 3 µl volume of testing liquids were used to eliminate gravity effects, and contact angle was measured after 3 s of placement droplet on the sample surface in order to reach thermodynamic equilibrium between the liquid and the sample interface. Minimum five readings were taken in order to calculate the average value and obtain standard deviation for the contact angle of each testing liquid. Surface free energy (γ_s), its polar (γ_s^p), and dispersive (γ_s^d) components (Equation (1)) were evaluated using

the SCA20 software through the application of the Owens-Wendt-Rabel-Kaelble regression model [34] by an application of a geometric mean (Equation (2)). The subsequent substitution in the Young equation (Equation (3)) can be used for obtaining a linear equation of the type $y = mx + c$ (Equation (4)), which was used for the evaluation of the surface free energy of the prepared and treated polymer nanocomposite samples:

$$\gamma_s = \gamma_s^p + \gamma_s^d \quad (1)$$

$$\gamma_{sl} = \gamma_s + \gamma_l - 2\sqrt{\gamma_s^d \gamma_l^d} - 2\sqrt{\gamma_s^p \gamma_l^p} \quad (2)$$

$$\gamma_s = \gamma_{sl} + \gamma_l \cos\theta \quad (3)$$

$$\frac{\gamma_l(1-\cos\theta)}{2\sqrt{\gamma_s^d}} = \sqrt{\gamma_s^p} \cdot \sqrt{\frac{\gamma_l^p}{\gamma_l^d}} + \sqrt{\gamma_s^d} \quad (4)$$

where (γ_s^p) and (γ_s^d) are the polar and dispersive parts of the surface energy of the solid (γ_s), respectively, and (γ_l^p) and (γ_l^d) are the polar and dispersive parts of the surface tension of the liquid (γ_l), respectively.

2.7. Surface morphology analysis

The surface morphology changes of plasma-treated and aged samples were investigated using scanning electron microscopy (SEM). SEM equipment Nova NanoSEM 450 (FEI, Hillsboro, OR, USA) was used for this purpose. A very thin Au layer (few nm) was sputter-coated on the sample surface to ensure a high resolution of resulting SEM images in 2D scale as elimination of electrons accumulation.

The detailed information about the surface topography of the PHBV samples in 3D scale was obtained using atomic force microscopy (AFM). An AFM device MFP-3D (Oxford Instruments Asylum research, Abingdon, Oxford, UK) using a silicon probe (Al reflex coated Veeco model – OLTESPA, Olympus, Tokyo, Japan) was employed to capture high-resolution AFM images (512×512 points) using a non-contact tapping mode in air under ambient conditions. First the homogeneity of different surface areas was checked by scanning of different surface areas, and then a representative high-resolution image was recorded and R_a value was evaluated. The surface roughness was evaluated by the R_a parameter considering the average height of irregularities relative to the sample surface in a perpendicular direction. Moreover, a line profile of the PHBV surface (z-axis) was evaluated from ZSensor.

2.8. Chemical composition analysis

Qualitative analyses of the chemical composition changes in the PHBV samples after plasma treatment and accelerated weathering were carried out by Fourier-transform infrared spectroscopy (FTIR) using an attenuated total reflectance accessory. An FTIR Spectrometer Frontier (PerkinElmer, MA, USA) was used for obtaining the spectra in the middle infrared region (4000–400 cm^{-1}) using a ZnSe crystal allowing ~1.66 μm penetration depth, using an average of 8 scans with a resolution of 4 cm^{-1}. Good contact between the analyzed samples and the crystal was ensured using a pressure clamp, allowing obtaining a high spectral quality.

2.9. Thermal analysis

The differential scanning calorimetry (DSC) analyses were performed using a DSC8500 (PerkinElmer, Waltham, MA, USA) differential scanning calorimeter. The plasma-treated PHBV samples (5–10 mg) were heated from 30 to 100 at 10 °C·min^{-1}. The melting enthalpies of PHBV were determined from the DSC curves. The degree of crystallinity for the PHBV and its composites was calculated according to Equation (5):

$$X_c\,[\%] = \frac{\Delta H_m}{\Delta H_m^0} \cdot 100 \quad (5)$$

where ΔH_m is the measured melting enthalpy, and ΔH_m^0 is the enthalpy of melting of the 100% crystalline polymer, with a value of 109.5 J·g^{-1} for PHBV [35]. The cooling scan was used to analyze ΔH_c, the enthalpy of crystallization, and a second heating scan (curves are not shown here) was used to analyze the glass transition temperature, T_g.

A TGA4000 (PerkinElmer, Waltham, MA, USA) thermogravimetric analyzer (TGA) was used to analyze the thermal degradation behavior of the samples. The analyses were done from 30 to 600 °C at a heating rate of 10 °C·min^{-1} under nitrogen flow (20 ml·min^{-1}). The sample masses were 10–15 mg.

2.10. Mechanical properties

An amplitude modulation–frequency modulation (AM–FM) technique was used for an evaluation of the mechanical properties of the PHBV samples in the top surface area using AFM. The AFM cantilever

with the tip is excited simultaneously at its fundamental resonant frequency and another eigenmode. The fundamental resonance is then used to obtain the topographical features of the PHBV samples, and the mechanical properties are analyzed by tracking the frequency and amplitude-shift of another eigenmode. The measured frequency shift Δf is then used for an evaluation of the interaction stiffness (Δk^{FM}) by Equation (6):

$$\Delta k^{FM} = 2k_c \cdot \frac{\Delta f}{f_c} \quad (6)$$

where k_c is the spring constant of the cantilever and f_c is the frequency of the eigenmode of the cantilever with the tip. In order to obtain Young's modulus of the measured samples, a general Hertz model was applied, describing the contact mechanics between the tip and the analyzed sample surface. A PHBV standard with a known Young's modulus (632.3 MPa) was first used for the calibration of the cantilever to determine its elasticity (42.04 kPa·Hz^{-1}). This elasticity was then used for obtaining the absolute values of Young's modulus of the analyzed samples. Gaussian fitting of the main peaks was then applied to obtain the mean values of Young's modulus presented in the related histograms.

The tensile properties were determined at room temperature in a Lloyd LR 50 k Plus (Lloyd Instruments, Ltd., Fareham, UK) universal testing machine at a stretching speed of 10 mm·min^{-1} (ASTM D638). The gauge length was 25 mm, and the sample (dumbbell shape) width and thickness were 3.25 and 1 mm, respectively. Five independent measurements were carried out for each sample in order to obtain an average value and standard deviation of mechanical properties.

3. Results and discussion

3.1. Plasma treatment optimization

The plasma treatment process was first optimized in terms of treatment time varying from 1 to 10 s and from 15 to 180 s for corona and RF plasma treatment, respectively. Static contact angle measurements were performed on PHBV samples. The contact angle analysis is a rapid, simple, and direct method to evaluate the wettability of the PHBV samples. The plasma method induces noticeable changes on the polymer surface even after a short treatment time. Figure 1 and Figure 2 show the effect of the plasma exposure time on the water, ethylene glycol, and formamide contact angles of plasma-treated PHBV samples in air. The pristine PHBV has a water contact angle of about 70°. As a result of the plasma irradiation, the water contact angle decreased after 1 s of corona treatment, but the lowest value was observed for an exposure time of 7 s. Similar to that, when the RF plasma was applied, the water contact angles dropped after 60 s of treatment and then slightly increased with a longer exposure time. It can be seen that both plasma treatments caused a marked decrease of water contact angle from 72.7±1.4° for untreated PHBV to 52.0±0.9 and 42.4±1.5°, within the 7 and 60 seconds, after corona and RF plasma treatment, respectively.

The reduction of the water contact angle suggests an obvious improvement of surface hydrophilicity, which is attributed to the cleavage of hydrophobic groups and the formation of new polar groups, OH, C=O,

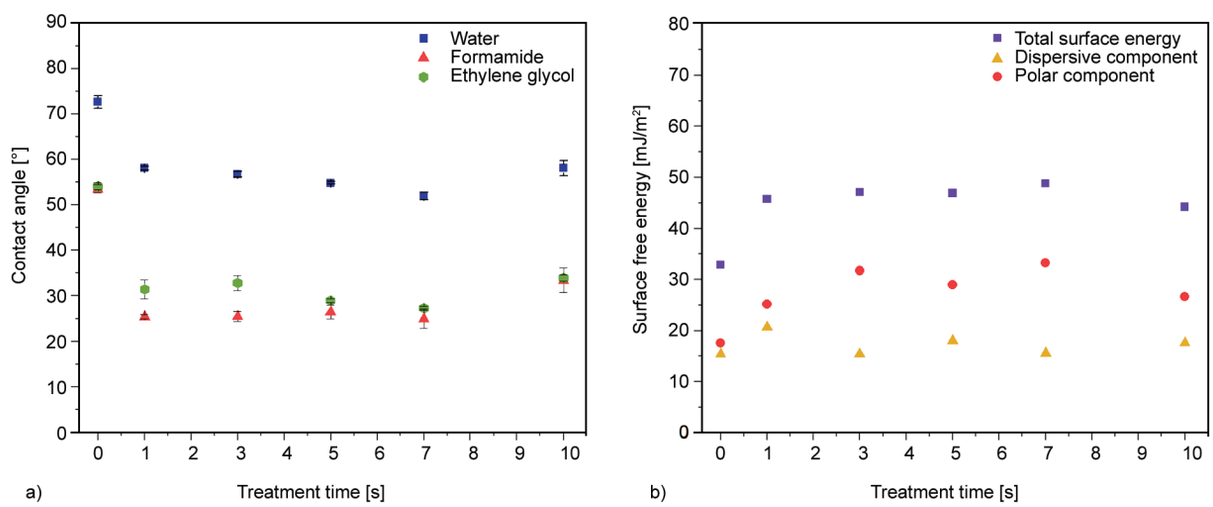

Figure 1. Contact angle (a) and surface free energy (b) of PHBV samples treated by corona plasma *vs*. treatment time.

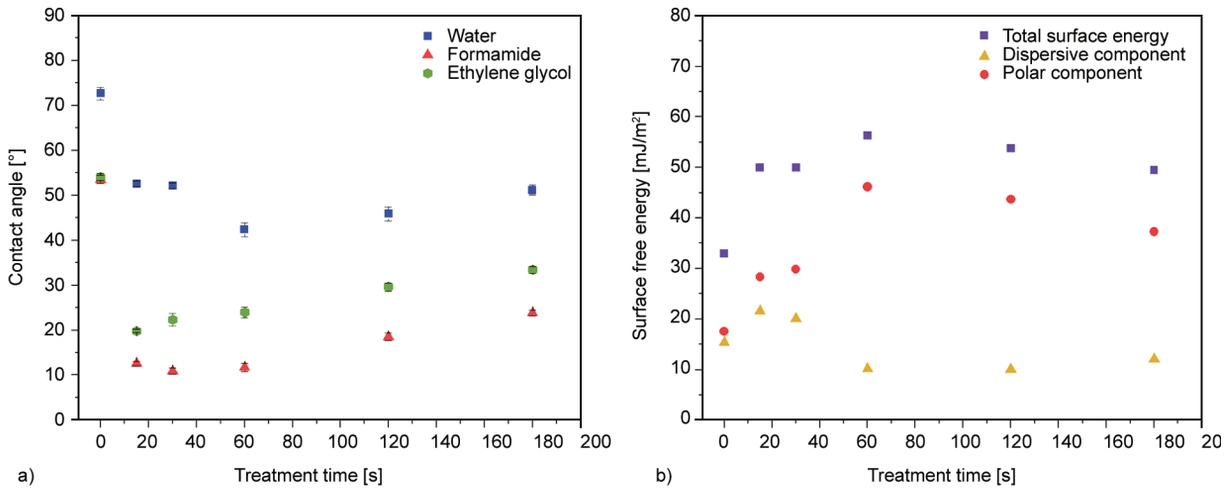

Figure 2. Contact angle (a) and surface free energy (b) of PHBV samples treated by RF plasma *vs*. treatment time.

and COOH, on the PHBV surface upon the plasma treatment [36]. Thereafter, the surface free energy slightly increased after plasma exposure reaching 48.79 and 56.4 mJ·m^{-2} for 7 and 60 seconds of corona and RF treatment, respectively.

These conditions were subsequently selected for treatment of the PHBV samples in order to perform accelerated weathering. Improved hydrophilicity of plasma-treated PHBV with enhanced water contact could potentially result in accelerated hydrolytic degradation of the PHBV.

3.2. Surface morphology characterization

The morphology of the samples before and after plasma treatment was analyzed by SEM.

Figure 3 shows the changes in the surface morphology of the PHBV samples treated with corona or RF, as well as their change over the time of weathering exposure. The neat PHBV presents a smooth morphology, which was also seen in the RF plasma treated samples, while corona treatment was responsible for a slightly rougher morphology. After 500 h of moisture and photo exposure, a noticeable corrugation on the surface of all the samples is noticeable, while it was more pronounced in the RF treated PHBV sample. This could have been caused by a more effective treatment of RF plasma compared to corona treatment, resulting in higher surface wettability with more susceptibility to hydrolysis during the weathering process. It is known that the amorphous regions of PHBV are able to transform into the crystalline state as a result of weathering [19]. Crystal occupies a smaller volume than the amorphous region, thus surface 'contraction' occurs, which leads to the formation of the rougher surface [37].

The SEM images indicate that the sample treated with corona showed significant changes in its surface morphology after exposure for 1000 h. There is a high roughness and some holes and cavities. Segregation is even more visible in the RF treated sample. Significant changes in the treated surface show that plasma had a significant effect on the degradation of the polymer surface, especially when compared to the untreated PHBV surface. Such characteristics were also observed for the PHBV samples after 2000 h of accelerated weathering exposure. Visible roughness and a large number of holes were present on the surface. The voids encourage hydrolytic and UV degradation to penetrate into the bulk. Thus, the water molecules (from the moisture present in the condensation step of the accelerated weathering) can diffuse, as well as the penetration of UV can occur simultaneously on the surface and in the bulk of the material. From these analyses, it can be clearly seen that the RF plasma treatment has the highest impact on an enhancement of the weathering degradation of the PHBV samples. Regarding the natural weathering exposure, all the samples exhibited more damaged surfaces than observed after accelerated weathering. The main reason can be related to the longer period of time during which the samples were exposed to humidity and UV. During artificial weathering, samples were exposed to 100% humidity only for 4 h, while during natural weathering, the samples were exposed to humidity 24 h per day despite the irregular level of moisture. The high level of humidity observed in the Middle East is a big issue as reported in several works that mainly focused on corrosion challenges for the oil and gas industry, thus authors were looking for a potential

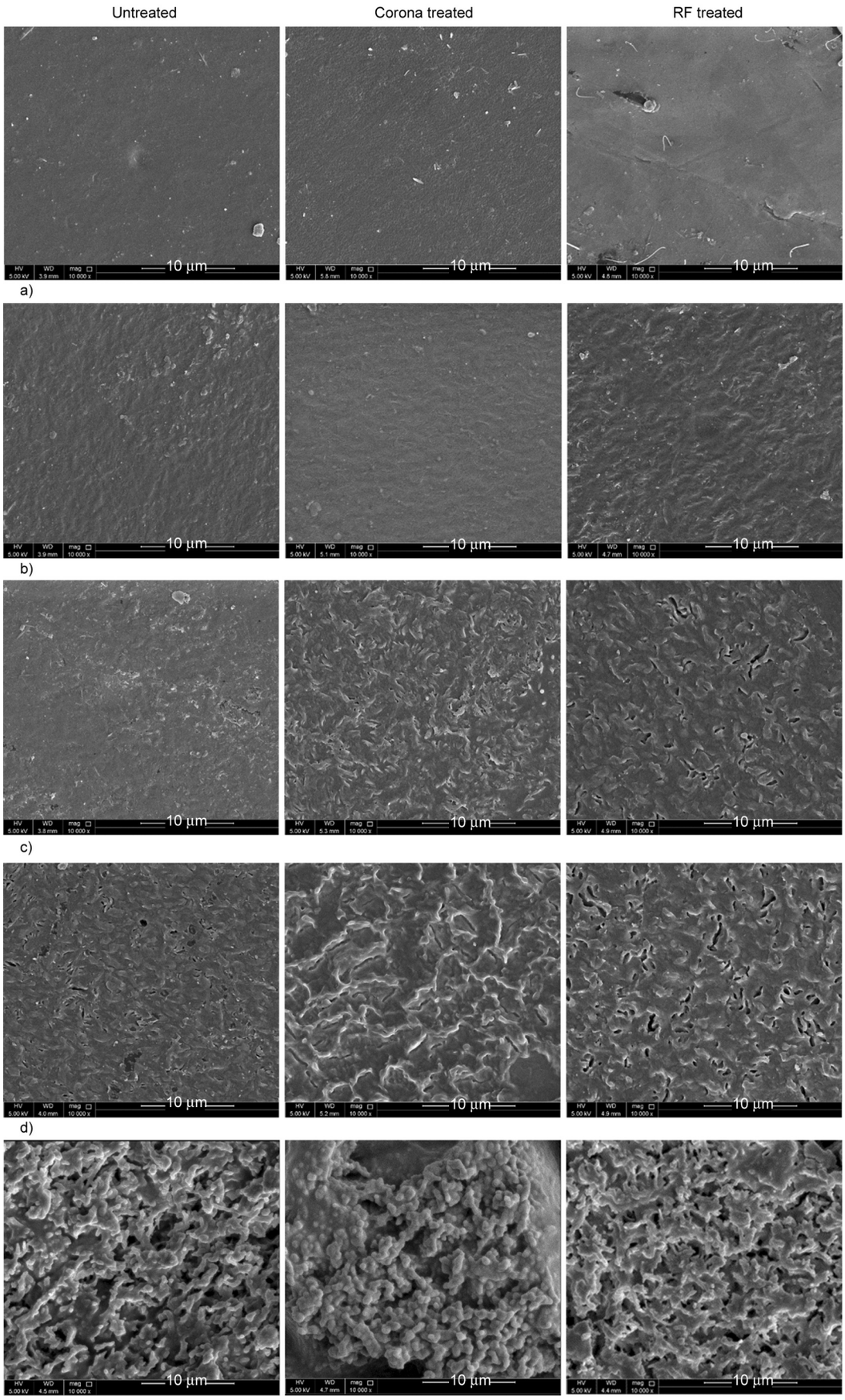

Figure 3. SEM images of PHBV samples (from left to right: untreated, corona and RF treated) before weathering (a), after accelerated weathering (b) 500 h; (c) 1000 h and (d) 2000 h, and after natural weathering (e).

combination of preventive or remediation strategies for extending the lifetime of materials [38]. In addition, the daylight exposure happened around 12 h per day instead of 8 h as simulated in the weatherometer. It should be noted that the direction of UV irradiation changed over the day according to the sun's position. Thus, the degradation process is much more intense, as also observed in the FTIR section.

The topographical structures and related line profiles of the PHBV samples obtained by AFM are shown in Figure 4. The untreated PHBV shows a relatively smooth surface area with relatively small roughness in line profile, while the R_a was 7.4 nm. Corona plasma treatment was responsible for significant roughness changes, while the R_a increased to 53.4 nm, while roughness in line profile increased significantly. On the other hand, RF plasma treatment did not affect the surface topography and the R_a had an identical value to that of the untreated PHBV. 500 h of accelerated aging resulted in a surface roughness increase for the untreated and RF plasma treated samples, while R_a was 18.9 and 35.9 nm, respectively. In the case of the corona-treated PHBV samples, the R_a value decreased to 20.8 nm, but topographical textural changes were observed. 1000 h of accelerated weathering led to an increase in the surface roughness for all the PHBV samples. 2000 h of accelerated weathering resulted in a significant surface roughness increase observed in line profile, while R_a was 109.6, 169.7, and 249.0 nm for the untreated, corona treated, and RF plasma-treated PHBV samples, respectively. Moreover, NW was responsible for the highest surface roughness increase for untreated and RF plasma-treated PHBV samples achieving R_a values equal to 135.2 and 265.1 nm, respectively. The obtained findings indicate that corona and RF plasma significantly affected the degradation process of the PHBV surface, while the RF plasma treatment effect was more pronounced.

3.3. Surface chemistry (FTIR)

The FTIR spectra of plasma-treated PHBV were measured in order to obtain qualitative information about the chemical composition, for the unaged as well as the aged samples under accelerated weathering up to 2000 h and 1 year (8760 h) of natural weathering (Figure 5 and Figure 6). The most important peaks in the IR spectra for PHBV are shown in two zones, *i.e.*, 1750–1700 and 1100–1260 cm^{-1}. The strong peak at 1750–1700 cm^{-1} is the result of C=O stretching vibrations associated with crystalline and amorphous carbonyl groups. The peaks in the region of 1100–1260 cm^{-1} are because of C–O stretching. The peaks at 1472, 1448, 1425, 1338, 1335 and 1313 cm^{-1} are due to the CH_2 and CH_3 asymmetric and symmetric deformations, as well as at 3000–2800 cm^{-1} assigned to the asymmetric and symmetric deformations in the methylene chains ($–CH_2–$). As a result of intermolecular H-bonded and O–H stretching modes, a broad feature is seen at ~3300 cm^{-1}. The key peaks of the C–C chains stretching mode are shown in the 1000–800 cm^{-1} spectral area [19, 39, 40].

All the samples exhibited the same characteristic bands, and only slight changes were found after accelerated weathering. In the PHBV/Corona/2000h and PHBV/RF/2000h spectra, a new shoulder in the range of 1580–1660 cm^{-1} is evident (indicated by a dashed circle in Figure 5 and Figure 6). The wide range is assigned to the overlapping of hydroperoxides and C=C double bonds in the newly formed chains due to the photodegradation of PHBV according to a Norrish II mechanism and the possible presence of absorbed water in the material after long periods of weathering involving condensation steps [19, 41–45]. On the other hand, the peak around 1525 cm^{-1} disappeared after weathering. Once radical sites were formed on the plasma-treated sample surface, secondary reactions can occur. The plasma treatment has a noticeable effect on the surface properties of the samples as a result of a combination of different processes such as ablation, etching, functionalization, and crosslinking processes [46, 47], as well as thermal and irradiation degradation [48]. According to Nabedryk and Breton [49], the ethylenic C=C stretching vibration is observed at 1527 cm^{-1}. Cools *et al.* [48] reveals some possible reactions occurring on plasma-treated samples, and $CH_2{=}CH_2$ can be a reaction product from that. The erosion process occurring during weathering and the degradation process itself should be enough to degrade the $CH_2{=}CH_2$ structures created on the PHBV/corona/0h and PHBV/RF/0h surface during the plasma treatment. In addition, it could be noted that the intensity of the bands placed at 1263 and 1226 cm^{-1} ascribed to the C–O–C stretching mode [50], clearly becomes weaker after long periods of weathering as observed for PHBV/RF/2000h. This result indicates the expected polymer chain scission of plasma-treated PHBV after weathering under hydrolysis and photodegradation.

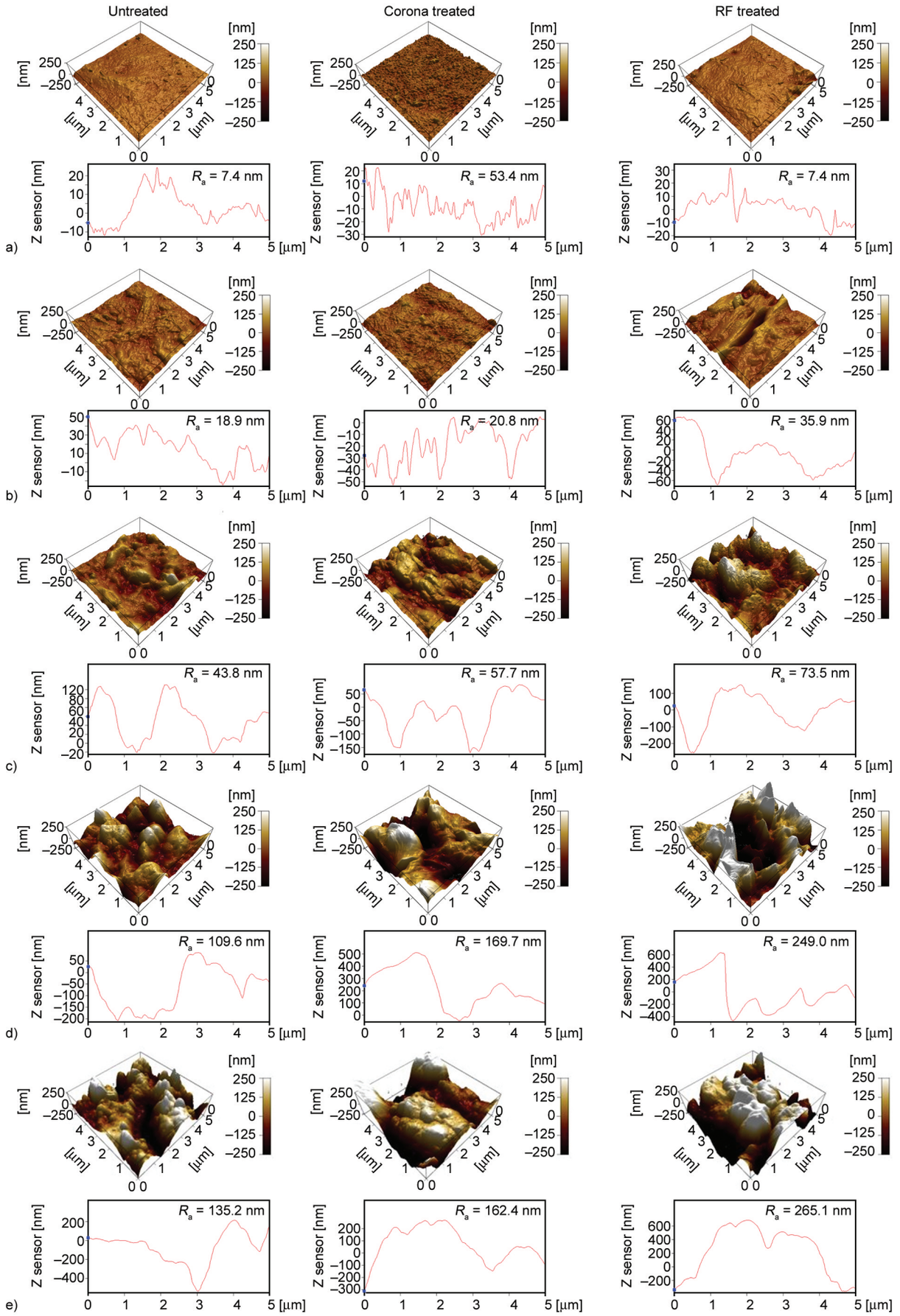

Figure 4. AFM images of PHBV samples (from left to right: untreated, corona and RF treated) before weathering (a), after accelerated weathering (b) 500 h; (c) 1000 h and (d) 2000 h, and after natural weathering (e).

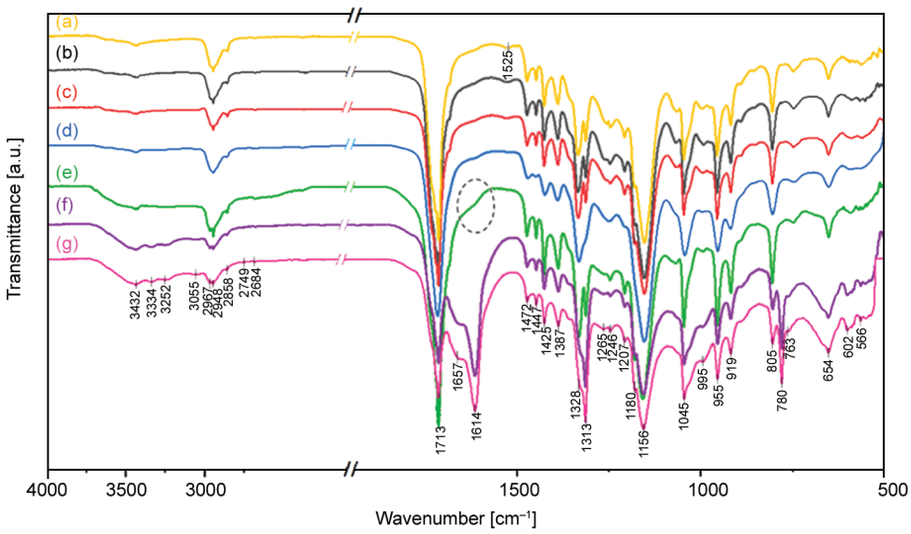

Figure 5. FTIR spectra of untreated and corona treated PHBV before and after natural and accelerated weathering: (a) PHBV/0h, (b) PHBV/Corona/0h, (c) PHBV/Corona/500h, (d) PHBV/Corona/1000h, (e) PHBV/Corona/2000h, (f) PHBV/NW and (g) PHBV/Corona/NW.

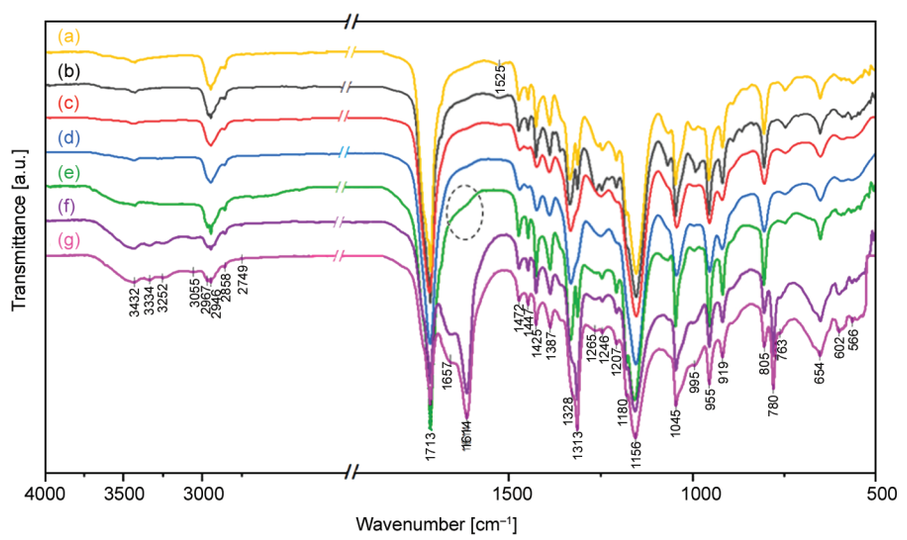

Figure 6. FTIR spectra of untreated and RF treated PHBV before and after natural and accelerated weathering: (a) PHBV/0h, (b) PHBV/RF/0h, (c) PHBV/RF/500h, (d) PHBV/RF/1000h, (e) PHBV/RF/2000h, (f) PHBV/NW and (g) PHBV/RF/NW.

The intensity and positions of the bands around 3000 and 3500 cm^{-1}, could also support this.

Regarding our previous work [19], FTIR results showed that photo and hydrolysis degradation of PHBV/2000h followed the same steps of the degradation noticed for plasma-treated samples. However, the typical photocleavage via Norrish II takes a pronounced place in natural weathering degradation, showing remarkable differences in the FTIR spectra of untreated and plasma-treated PHBV. The intensity of peak associated with C=O in the carboxylic group at 1713 cm^{-1} decreased as a result of degradation processes. Moreover, the large absorptions and well-defined peaks at 1657, 1614, 1313, and the new one at 780 cm^{-1} suggest an abundance of unsaturated vinyl, ketones, aldehydes, and carboxylic acid salts subsequent from the formation of a hydroperoxide derivative during photooxidation and their subsequent degradation as a result of the simultaneous occurrence of several chemical mechanisms [19, 41, 51–53].

3.4. Wettability analysis

In order to assess the effects of plasma treatment on the weathering degradation of PHBV, contact angle measurements were carried out. Figure 7 and Figure 8 show the contact angle results of water, formamide, and ethylene glycol for the plasma-treated PHBV as

a function of accelerated and natural weathering time. The contact angles of different testing liquids were then used for an evaluation of the surface free energy and its polar and dispersive components. The PHBV showed a higher value of contact angle for water, 72.7±1.4° [19], compared to the plasma-treated PHBV samples. The lowest value for contact angle for water was obtained for PHBV/RF/0h, 42.4±1.5°, while PHBV/Corona/0h achieved 52.0±0.9°. This reduction in the contact angle indicating an increase in the hydrophilicity was mainly caused by a formation of the polar functional groups formed by the plasma treatment, as previously mentioned, although significant differences were not found in the FTIR spectra. This was probably caused by the high penetration depth of the infrared beam (~1.66 μm) in comparison with only a few tens nm plasma treated layer.

The surface free energy was evaluated by Owens-Wendt-Rabel-Kaelble method. The surface free energy of the PHBV/Corona/0h sample was 48.8 mJ·m^{-2}, which can be separated into its two components: the polar component with a relatively high value of about 33.2 mJ·m^{-2} and the dispersive contribution with a low value of 15.6 mJ·m^{-2}. As expected from the contact angle values, the surface free energy and its polar component obtained for PHBV/RF/0h achieved the highest values, *i.e.*, 56.4 and 46.1 mJ·m^{-2}, respectively.

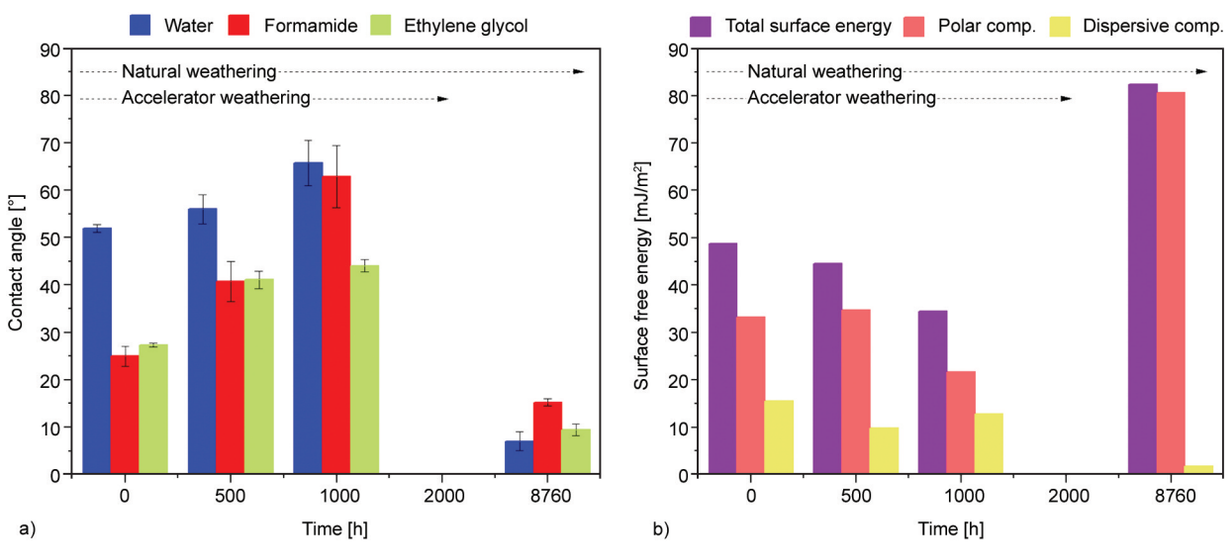

Figure 7. Contact angle (a) and surface free energy (b) of PHBV samples treated by corona plasma *vs*. accelerated (500 and 1000 h) and natural (8760 h) weathering time.

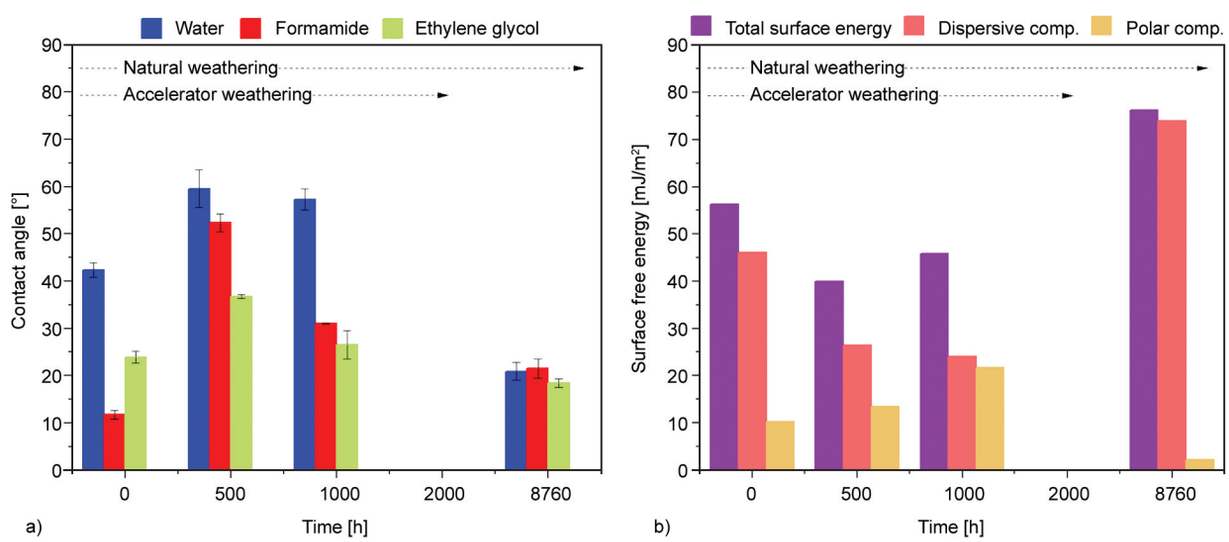

Figure 8. Contact angle (a) and surface free energy (b) of PHBV samples treated by RF plasma *vs*. accelerated (500 and 1000 h) and natural (8760 h) weathering time.

Regarding the effect of accelerated weathering, a decreasing wettability tendency is observed with increasing weathering exposure. Polar groups on the polymer surface promote the degradation of the polymer since it could be easier hydrated. Results of the hydrolysis are cleavage of ester bonds and, consequently, chain scission. Plasma activation leads to degradation in the surface layers of the material, and the UV attack occurs simultaneously to form compounds containing terminal carbonyl groups, as noticed in FTIR. As shown in Figure 3, a rough surface was noted for all the samples after 500 h of weathering, but much more pronounced in the PHBV/RF/500h sample. Thus, it was clear that RF plasma activation accelerated degradation. PHBV/Corona/500h was more stable to degradation reactions. Less effective plasma activation or some crosslinked surface occurred during the plasma treatment and could justify the similar polar component observed in PHBV/Corona/0h and PHBV/Corona/500h. Thus, the observed increase in contact angle for water to 56.0±3.1° only occurred due to the observed physical modifications of the surface.

It is more likely that during activation, polar groups and low-molecular products from the surface of samples are cleaved, resulting in increased roughness and lower surface energy values than the previous results. The increase of surface roughness did not favor the wettability of the PHBV/Corona once the PHBV/Corona/1000h was more hydrophobic, in contrast with the argument by Yang *et al*. [54] showing that the increase in roughness is one of the reasons for the increase in hydrophilicity in plasma-treated samples. This could probably be explained by the Cassie-Baxter model, where trapped air within small voids caused lower wettability [55]. The CA of corona and RF plasma-treated PHBV could not be determined after 2000 h because the surfaces were completely degraded as observed in Figure 3, thus it was not possible to correctly assess this value. This behavior was also observed in our previous work for neat PHBV [19]. The dispersive component of the surface energy contribution increases gradually as the accelerated weathering time increases for the RF plasma-treated samples. The surface free energy showed a remarkable increase, from low values of 40.0 $mJ \cdot m^{-2}$ for the PHBV/RF/500h sample up to values of 45.9 $mJ \cdot m^{-2}$ for PHBV/RF/1000h. The dispersive component clearly depends on the roughness of the samples resultant from degradation, and it promotes the deeper degradation of the sample. Similar behavior was noted for PHBV after accelerated weathering [19].

Remarkable results were found after natural weathering, *i.e.*, after 8760 h of outdoor exposure. Both plasma-treated PHBV samples showed a very low contact angle for water, formamide, and ethylene glycol, as shown in Figure 7 and Figure 8. For PHBV/NW the contact angles for the three liquids were 7.6 ± 0.7, 18.7 ± 2.0, and 12.5 ± 3.6°, respectively. The combination of several factors promotes the observed results. The cleavage of ester linkages during weathering exposure results in shorter polymer chains. Thus, shorter polymer chains are easily able to reorganize into crystalline domains (as will be discussed in the DSC section), which results in a closed structure for water absorption. In addition, the SEM and AFM analyses even showed an increase in roughness, which can also contribute to an increase in the water contact angle of the PHBV samples for water. Besides the proposed physical changes in the sample surfaces, the chemical modification also occurred. The density of the polar and non-polar species, such as carboxylic and hydroxyl end groups but also C=C linkages, also balanced the contact angle values, which is corroborated with the FTIR analysis. Moreover, the decrease in contact angles could be explained by Wenzel wetting theory [55], while the internal larger voids and surface defects can be wetted too.

3.5. Thermal properties

DSC analysis shows several changes during the first heating, and cooling cycles associated with weathering exposure of plasma treated PHBV samples (Figure 9 and Figure 10). DSC analysis was used to determine the changes in the degree of crystallinity characterized by enthalpy and melting phenomena of PHBV samples before and after 500, 1000, and 2000 h of accelerated weathering and also after natural weathering exposure. The thermal parameters from the first heating and cooling scans (melting and crystallization temperatures and enthalpies, respectively, T_m, T_c, ΔH_m and ΔH_c), as well as the degree of crystallinity (X_c) are summarized in Table 1. In addition, a second heating scan (not shown here) was used for the identification of the glass transition (T_g).

A large endothermic event, ranging from 80 to 95 °C, was observed in both the case of PHBV/Corona/0h and PHBV/RF/0h, as well as a small endothermic

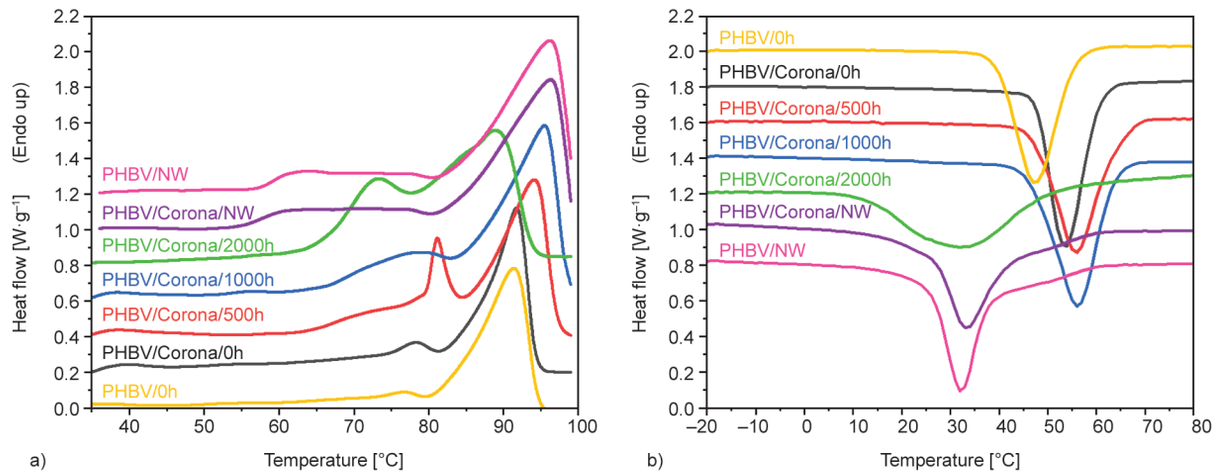

Figure 9. DSC first heating (a) and cooling (b) curves of PHBV and corona treated PHBV samples before (0 h) and after accelerated (500, 1000, and 2000 h) and natural weathering.

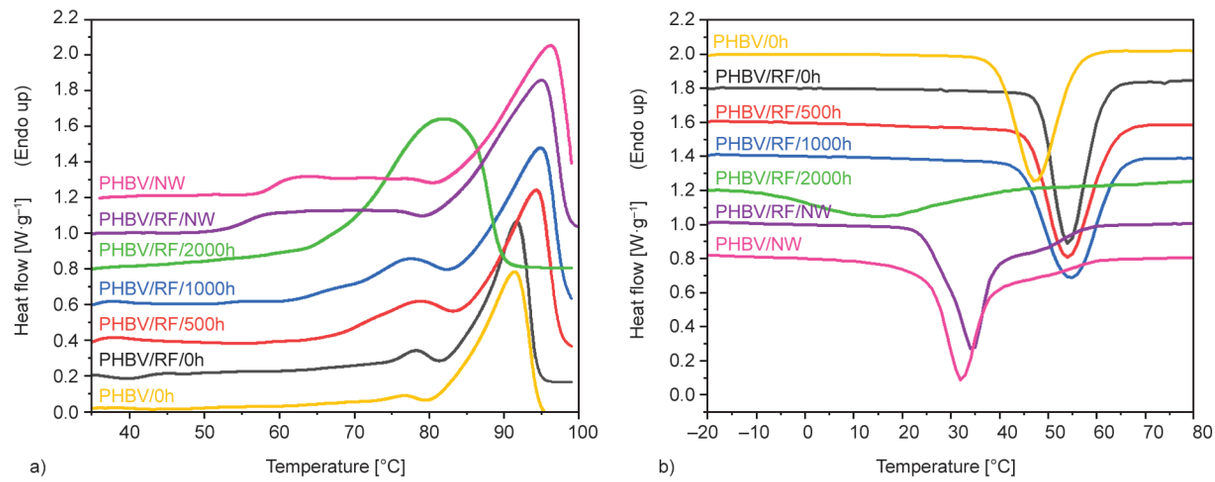

Figure 10. DSC first heating (a) and cooling (b) curves of PHBV and RF treated PHBV samples before (0 h) and after accelerated (500, 1000, and 2000 h) and natural weathering.

Table 1. DSC data obtained for PHBV samples and PHBV samples treated by corona and RF plasma before and after weathering.

Sample	1st heating			Cooling		2nd heating	
	ΔH_m [J·g^{-1}]	T_{m1} [°C]	T_{m2} [°C]	ΔH_c [J·g^{-1}]	T_c [°C]	T_g [°C]	X_c [%]
PHBV	58.8	76.6	91.5	47.0	47.5	–47.3	53.7
PHBV/NW	60.3	56.8–80.9	96.4	33.4	52.3	–41.7	55.1
PHBV/Corona/0h	36.3	78.3	91.9	–42.05	53.6	–44.0	33.2
PHBV/Corona/500h	60.4	80.9	94.4	–45.36	56.0	–43.8	55.2
PHBV/Corona/1000h	63.7	77.1	95.8	–50.49	56.3	–42.4	58.2
PHBV/Corona/2000h	73.2	72.5	88.8	–37.51	31.2	–42.3	66.8
PHBV/Corona/NW	64.9	52.2–80.7	96.5	51.3	32.1	–41.0	59.3
PHBV/RF/0h	36.9	78.5	91.1	–42.35	54.3	–44.1	33.7
PHBV/RF/500h	60.7	77.9	94.5	–45.47	54.0	–43.0	55.4
PHBV/RF/1000h	62.2	77.3	95.2	–47.39	54.9	–43.0	56.8
PHBV/RF/2000h	83.7	81.5		–26.85	15.1	–43.1	76.4
PHBV/RF/NW	65.4	48.1–79.4	95.1	51.8	34.4	–40.9	59.8

peak a couple of degrees before 80 °C. This double melting peak also noted for untreated PHBV is commonly attributed to the presence of more than one crystallographic form, as well as to changes in the lamellar thickening and crystal perfection. Some authors also attributed it to melting, recrystallization, and re-melting processes [19, 39, 56, 57]. A single crystallization peak (T_c) was noticed during cooling at 54 °C for both samples before weathering, and the degree of crystallinity reached 33%. A similar profile was previously reported for neat PHBV [19], but a lower melting temperature and glass transition and a higher degree of crystallinity were noted for the untreated sample. The plasma treatment of a polymer can lead to several modifications in the surface by a combination of different physical processes, as previously mentioned, like ablation and etching of the surface area, but also chemical changes such as grafting, polymerization, crosslinking or functionalization [46, 47, 58]. Thus, the observed changes in DSC data after plasma treatment can be explained by a combination of these processes. First of all, the plasma discharge creates radical sites on the surface of the PHBV sample. Their oxidation upon exposure to ambient oxygen creates oxygen-containing groups, increasing the oxygen concentration on the surface. In addition, free radicals are also available for crosslinking reactions, which restricts the chain mobility and increases T_m and T_g of the plasma-treated PHBV [3, 59–61]. Moreover, it is known that the amorphous regions of PHBV are able to transform into crystalline domains as a result of chain scission and the ability of the shorter chains to self-re-organize. Thus, it was expected to observe some increase in the degree of crystallinity of plasma-treated PHBV. However, the opposite was noted, and the X_c for PHBV/ Corona/0h and PHBV/RF/0h decreased from 54% for neat PHBV to around 33% after plasma treatment. The shorter polymer chains are probably more susceptible to be removed by the vacuum system, as well as other degradation products from the plasma treatment, resulting in a selective ablation of the surface, which may cause the observed fluctuations in the degree of crystallinity [37, 59].

Slight changes were observed in PHBV/Corona and PHBV/RF after 500 and 1000 h of the accelerated weathering exposure. Whereas the T_g and T_{m1} showed some fluctuations for PHBV/Corona, the central peak around –43 and 78 °C, respectively, remained constant for PHBV/RF. Both plasma-treated samples showed increased T_{m2} after these periods of time, resulting from the chain scission of PHBV during degradation and the gradual increase in crystallinity, which hinders the polymer mobility under melting conditions. The double melting peak of PHBV/Corona/2000h shifted to lower temperatures, 73 and 89 °C. Since the crystallinity degree did not decrease after 2000 h, this result reveals the continuous degradation of the amorphous phase of PHBV to rearrange into smaller size crystalline regions, giving rise to the observed lower T_{m1} and T_{m2}. The untreated PHBV presents similar behavior [19]. In the case of PHBV/RF/2000h several changes were observed. The first melting peak, usually associated with less perfect, smaller crystals, became larger than the second melting peak of the unweathered sample, while the higher-temperature peak disappeared. According to some authors [62] the low-temperature peak is usually considered the true melting peak. Thus, it develops as the crystallinity increases.

A clear crystallization peak was observed in the cooling scan for both plasma-treated PHBV. The temperature varies in a small range, from 54 °C for PHBV/Corona/0h to 56 °C for PHBV/Corona/1000h and from 54 °C for PHBV/RF/0h to 55 °C for PHBV/RF/1000h. The T_c dropped after 2000 h, and the lowest value was 15 °C observed for PHBV/RF/2000h, which is in accordance with the more prominent changes observed for this sample during the first heating scan. Similar to previously reported [19], the presence of polymer chains characterized by different molecular weights and different lengths results in a wider melting or crystallization temperature range. When crystallization occurs over a broader temperature range, it means that the degradation process reduces the rate of crystallization of PHBV, affecting the morphologies of its crystals.

Under natural weathering, there was a noticeable increase of X_c for all the samples achieving values similar to 1000 h of accelerated weathering exposure, as well as T_{m2} which remains fairly similar to 1000 h of accelerated degradation. Indeed, the results indicate a decrease of T_g with natural weathering for untreated and plasma-treated samples, which is more pronounced for PHBV/RF/NW. The decrease in T_g is explained by the decrease in the number-average molecular weight of the exposed samples, such confirmed by the large temperature range of the T_{m1} peak, which confirms a large number of shorter chains. The DSC results, therefore, suggest that RF

plasma treatment had a stronger influence on the degradation of PHBV under hydrolysis and photodegradation conditions from accelerated and natural weathering exposure.

3.6. Thermogravimetric analysis (TGA)

The influence of the plasma treatment on the thermal behavior of PHBV after accelerated and natural weathering exposure was investigated by TGA. The temperature corresponding to the 5 and 50% of mass loss during the thermal decomposition process ($T_{5\%}$ and $T_{50\%}$), and the temperature corresponding to the maximum mass loss rate (T_{max}), were determined from the thermogravimetric curves for corona and RF plasma-treated PHBV and collected in Table 2. As evidenced in Figure 11 where the thermogravimetric curves are reported, the mass loss takes place in one step for all the weathering times.

The thermal degradation of corona-treated PHBV consists of the main degradation step between 300 and 425 °C, with a maximum mass loss around 403 °C. Interestingly, PHBV/Corona/2000h shows a gradual decrease in mass starting at very low temperatures. One possible explanation for this behavior can be that some moisture from the condensation cycle remained on the PHBV surface. In addition, the main degradation step started around 200 °C but ended in the same temperature range as the other samples. It seems the PHBV/Corona/2000h present two degradation stages as usually noted in blends. The result can be attributed to the presence of the reactive species on the surface, which promoted the weathering degradation after 1000 h. However, 2000 h of hydrolysis and UV exposure was not enough for an equal surface and bulk degradation. The corona plasma treatment was not effective in enhancing the complete PHBV degradation in this period of time, which reduced the thermal stability of only part of the polymer.

The PHBV/RF samples exhibited the same profile as the PHBV/Corona samples, *i.e.*, one degradation step occurring between 300 and 425 °C, but a slight decrease from 409 to 406 °C was observed for T_{max} up to 1000 h of weathering. As known, plasma treatment affects the PHBV surface due to the radicals, excited atoms, and charged particles that are generated during this treatment promoting the wettability of PHBV resultant from chemical and physical modifications. Although the PHBV/RF showed good thermal stability, a significant change occurred after 2000 h of

Table 2. Characteristic degradation temperatures for untreated PHBV samples and PHBV samples treated by corona and RF plasma before and after weathering.

Sample	$T_{5\%}$ [°C]	$T_{50\%}$ [°C]	T_{max} [°C]
Untreated PHBV	348	398	407
PHBV/NW	349	402	406
PHBV/Corona/0h	349	396	403
PHBV/Corona/500h	352	398	404
PHBV/Corona/1000h	347	397	406
PHBV/Corona/2000h	272	394	404
PHBV/Corona/NW	332	396	405
PHBV/RF/0h	354	401	409
PHBV/RF/500h	354	400	407
PHBV/RF/1000h	339	397	406
PHBV/RF/2000h	324	364	370
PHBV/RF/NW	349	402	409

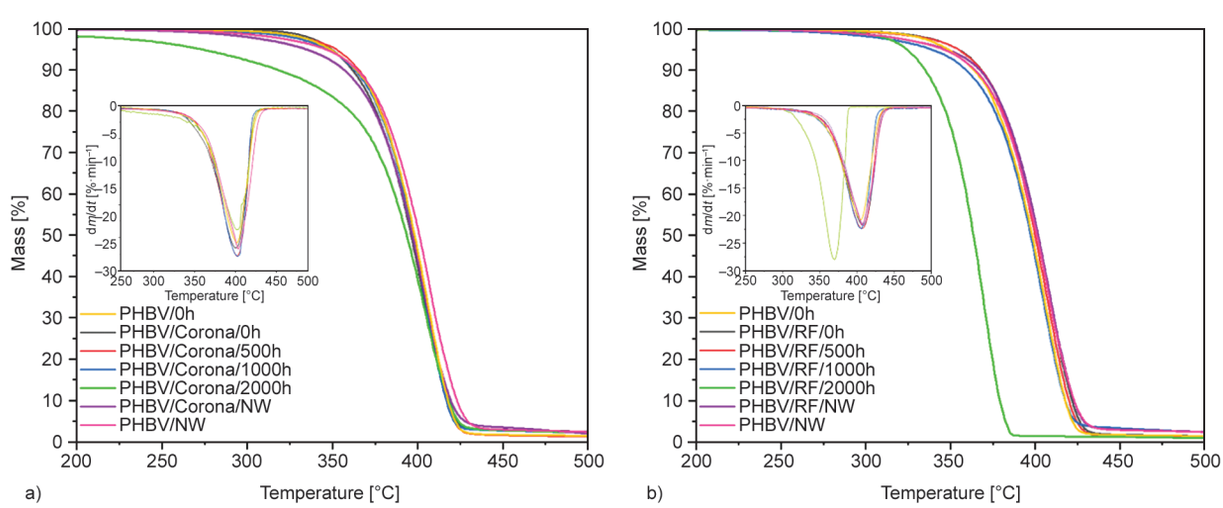

Figure 11. TGA curves of PHBV samples treated by corona (a) and RF (b) plasma before (0 h) and after natural and accelerated (500, 1000 and 2000 h) weathering.

weathering. A decrease in maximum degradation temperature was observed, reaching the lowest value of 370 °C, probably due to the molecular weight decrease after weathering. It seems to have already started in PHBV/RF/1000h as noticed from the values of $T_{5\%}$, decreasing from 354 to 339 °C. The weathering degradation occurred on the surface and in bulk due to the observed holes noted in the SEM images, which promoted the water diffusion and UV penetration during weathering from the surface to the deeper bulk.

Similar to the corresponding PHBV/Corona sample, this suggests higher hydrolysis and UV sensitivity for RF plasma-treated PHBV, which may be considered as a measure of the thermal stability, as well as the weathering degradation rate. On the other hand, as observed from $T_{50\%}$ and T_{max}, the degradation caused by natural weathering did not seem to affect the thermal stability of PHBV and the plasma-treated samples. These results confirm the trend observed using FTIR and DSC techniques, *i.e.*, one year of natural weathering exposure in the Middle-East environment provides a large range of different polymer chain sizes, but this time it was not enough to lead to the same degradation products of the 2000 h under accelerated weathering samples (with and without plasma treatment).

3.7. Mechanical properties

The mechanical properties of the PHBV samples in the top surface area were analyzed using an advanced AM–FM AFM technique, while Young's modulus distribution in the entire surface area was obtained. The AM–FM AFM images of the PHBV samples before and after accelerated and natural weathering are shown in Figure 12, and Young's modulus values (mean) are summarized in Table 3. The mean value of Young's modulus for the PHBV sample was 177.7 MPa. Corona plasma treatment noticeably decreased the mechanical properties of the PHBV sample, while RF plasma treatment was responsible only for a variable increase in Young's modulus. The mean value of Young's modulus of the PHBV/Corona/0h and PHBV/RF/0h samples was 141.7 and 179.0 MPa, respectively. The accelerated weathering aging led to Young's modulus changes as a result of a combination of thermal, UV, and hydrolytic degradations. 500 h of accelerated aging time resulted in an increase in Young's modulus values of all the PHBV samples as post-chemical processes. The mean values of the PHBV/500h, PHBV/Corona/500h, and PHBV/RF/500h were 276.7, 235.4, and 336.6 MPa, respectively. The additional accelerated weathering time led to an increase in Young's modulus for the untreated and corona-treated PHBV samples, whereas Young's modulus of PHBV/RF/1000h achieved the lowest value (108.8 MPa). 2000 h of accelerated weathering was responsible for lower mean values of Young's modulus of the plasma-treated PHBV samples in comparison with the PHBV samples after 500 h of accelerated weathering, while the untreated PHBV samples achieved even higher values of Young's modulus. This confirms the enhanced degradation of the plasma-treated PHBV samples caused by the polar functional groups susceptible to catalytic hydrolytic degradation together with UV and thermal degradation after longer weathering times. Natural weathering revealed lower mean values of Young's modulus for PHBV/NW (281.7 MPa) and PHBV/Corona/NW (171.1 MPa) in comparison with the sample after 2000 h of the accelerated weathering. The PHBV/RF/NW sample achieved remarkably higher mean values of Young's modulus (358.8 MPa). However, from the histogram, a double peak is clearly seen with the highest peak width distribution indicating different degradation degrees in different surface areas.

The tensile strengths of PHBV subjected to corona and RF plasma treatment are shown in Table 4. The initial tensile strength (σ_{break}) of the tested PHBV samples was 34.2±1.7 MPa, while Young's modulus (E), and elongation at break (ε_{break}) had values of 182±6 MPa, and 730±40%, respectively [19]. Since the plasma surface treatment does not affect the bulk of the unweathered samples, these values were similar for plasma-treated PHBV as shown in Table 4. A large drop in the mechanical properties was observed after 500 h of accelerated weathering. The tensile strength was 3.7±1.3 and 5.8±1.5 MPa, with respect to the corona and RF treatments. The results indicate a large decrease in the elongation at break as was noted for tensile strength, giving values of 3.9±1.8 and 3.3±1.3% for corona and RF samples. Moreover, a small decrease to 154±84 MPa for Young's modulus values was noted in the corona sample, whereas a slight increase to 278±51 MPa was achieved for PHBV/RF/500h. Similar behavior was already noticed for the untreated PHBV [19].

These properties are determined by the ratio of flexible and rigid characteristics from amorphous and

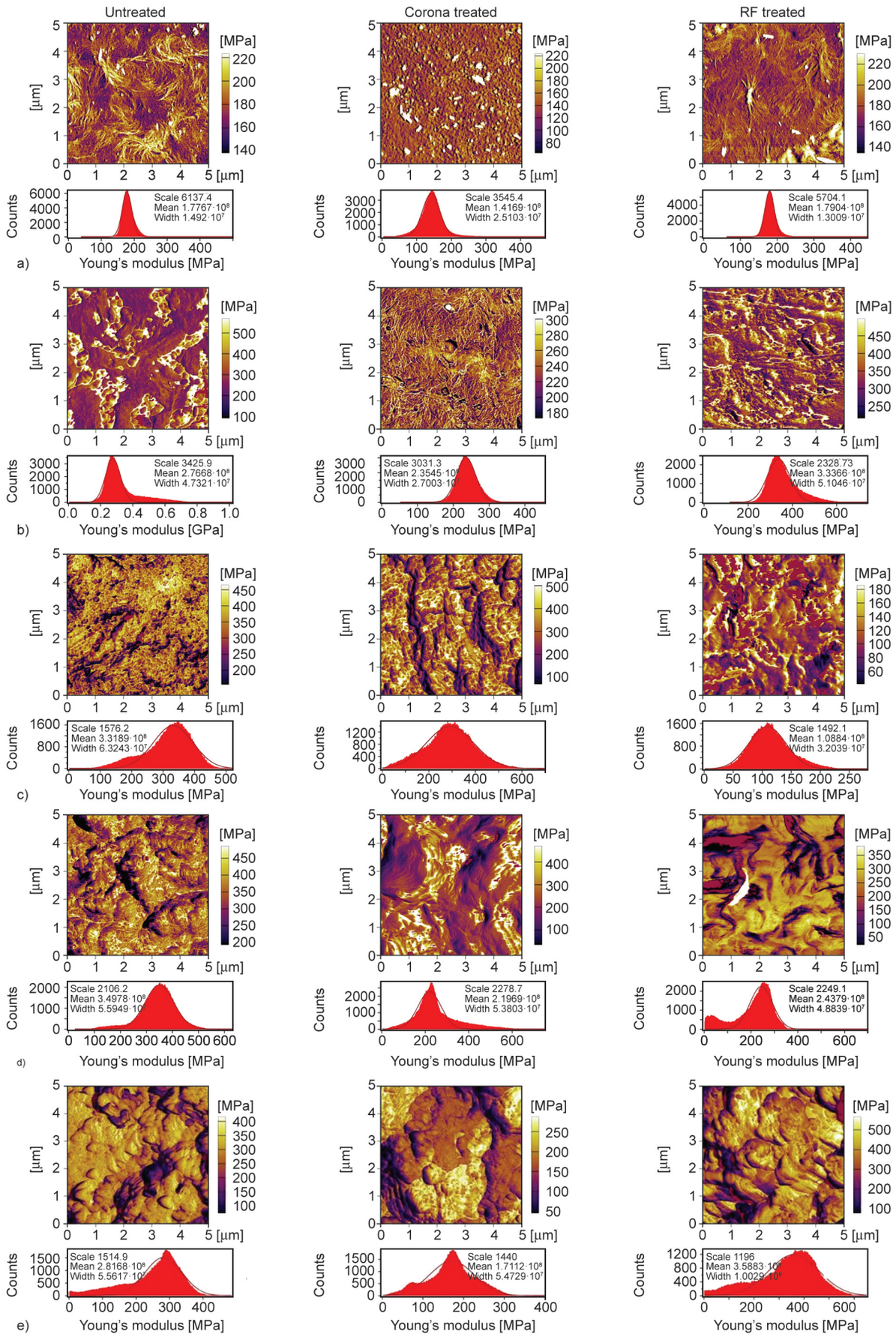

Figure 12. AM-AFM images of PHBV samples (from left to right: untreated, corona and RF treated) before weathering (a), after accelerated weathering (b) 500 h; (c) 1000 h and (d) 2000 h, and after natural weathering (e).

Table 3. Mechanical properties of the PHBV samples in the surface area before and after weathering.

Sample	Young's modulus [MPa].	
	Mean	Width
PHBV/0h	177.7	14.9
PHBV/500	276.7	47.3
PHBV/1000	331.9	63.2
PHBV/2000	349.8	55.9
PHBV/NW	281.7	55.6
PHBV/Corona/0h	141.7	25.1
PHBV/Corona/500h	235.4	27.0
PHBV/Corona/1000h	291.1	101.9
PHBV/Corona/2000h	219.7	53.8
PHBV/Corona/NW	171.1	54.7
PHBV/RF/0h	179.0	13.0
PHBV/RF/500h	336.6	51.0
PHBV/RF/1000h	108.8	32.0
PHBV/RF/2000h	243.8	48.8
PHBV/RF/NW	358.8	100.2

Table 4. Mechanical properties of the PHBV samples treated by corona and RF plasma before and after weathering.

Sample	σ_{break} [MPa]	ε_{break} [%]	*E* [MPa]
PHBV	34.2±1.7	730±40	181±6
PHBV/NW	N.A.	N.A.	N.A.
PHBV/Corona/0h	28.3±6.8	626±79	188±14
PHBV/Corona/500h	3.7±1.3	3.9±1.8	154±84
PHBV/Corona/1000h	1.0±0.7	1.3±0.6	75±21
PHBV/Corona/2000h	N.A.	N.A.	N.A.
PHBV/Corona/NW	N.A.	N.A.	N.A.
PHBV/RF/0h	20.5±15.7	631±130	190±18
PHBV/RF/500h	5.8±1.5	3.3±1.3	278±51
PHBV/RF/1000h	0.7±0.2	0.9±0.9	51.2±3
PHBV/RF/2000h	N.A.	N.A.	N.A.
PHBV/RF/NW	N.A.	N.A.	N.A.

N.A.: Not available

crystalline domains of the PHBV, which are degraded under moisture and UV attack. DSC analysis showed a significant increase in the crystallinity of the RF sample, which explains the observed increase of *E* after 500 h. The continuing reduction in mechanical properties after 1000 h is related to the continued degradation of the PHBV matrix involving changes in the molecular weight and phase morphology. When the plasma-treated PHBV samples are exposed to the action of moisture and UV light, hydrolysis and photodegradation processes take place. The enhanced hydrophilic PHBV surfaces modified by corona and RF plasma treatment promote their wettability during the condensation cycle of the accelerated weathering conditions. Chain scission of the PHBV chains occurs since, at the same time, they are attacked by UV-light. Fundamentally, a photodegradation via Norrish II mechanism happens, involving free radicals. These radicals may undergo several reaction paths to yield further radicals, together with oxygenated species such as hydroperoxides, ketones, and esters, as confirmed by FTIR. The result is a gradual decrease in the chain length of the PHBV from transforming the amorphous phase into a crystalline phase as a result of the re-organization of the resultant shorter chains, as noted after 500 h, as a higher fragility, lower tensile strength, and higher *E*. After 1000 h of exposure, the degradation proceeds, and the observed cracks and holes in the SEM images are responsible for promoting UV and water penetration to attack the bulk of the PHBV/Corona and PHBV/RF samples. The degradation process involves predominantly the destruction of the amorphous phase but also the crystalline regions. These reasons should explain the slight decrease noted in *E* values for both samples after 1000 h, but also for untreated PHBV. The PHBV/Corona/2000h and PHBV/RF/2000h samples, as well as untreated and treated PHBV samples after natural weathering, were not tested because they were significantly cracked and brittle.

From Table 4 it can be deduced that weathering exposure has a severe effect on the mechanical properties of the PHBV samples, whatever the plasma treatment or weathering type. However, RF samples showed to be significantly affected earlier by weathering conditions than corona samples. Thus, RF plasma was revealed to be an efficient treatment for surface modification promoting the degradation of PHBV material significantly.

4. Conclusions

The effect of the PHBV surface modification by corona and RF plasma treatment on the accelerated and natural weathering degradation was explored. Plasma treatments physically and chemically changed the surface of the PHBV samples. SEM observations show that plasma processing promotes the development of a rough surface and the formation of pores in the surface of PHBV after weathering. A decrease in the water contact angles and increase in surface

energy indicates the effectiveness of plasma treatment changing the hydrophobic character of PHBV due to the increase in the number of polar groups on the surface after oxidation of the free radicals achieved by plasma. FTIR spectroscopy displays the characteristic bands of PHBV, and a new event was noted indicating the hydration of samples and the C=C bonds created during photodegradation via a Norrish II mechanism. Structural analysis revealed an increase in the crystallinity degree resulting from the re-organization of the small chains originated during the weathering degradation, which was also confirmed by the shift in the melting and crystallization temperatures to lower values after weathering. The mechanical properties were significantly changed as a result of the weathering degradation. The improved wettability of the plasma-treated surfaces enhanced the water contact during the condensation cycle of the accelerated weathering test, giving rise to cavities and voids, which promote the water and UV attack of the PHBV bulk. In addition, the thermal stabilities were also slightly changed in plasma-treated PHBV. It is important to highlight that this was more evident in RF than corona-treated PHBV. Linking these results suggests that RF plasma treatment is an effective plasma method to improve the wettability of PHBV, which is the main cause of the earlier weathering degradation of PHBV in this study. In addition, the results seem to show that 1000 h of accelerated weathering exposure tends to equal the degradation products of one year of natural weathering exposure under the Middle-East environment.

Acknowledgements

This publication was supported by the Qatar University Collaborative Grant No. QUCG-CAM 19/20-3. The findings achieved herein are solely the responsibility of the authors. SEM analysis was accomplished in the Central Laboratories unit, Qatar University.

References

[1] Badia J. D., Kittikorn T., Strömberg E., Santonja-Blasco L., Martínez-Felipe A., Ribes-Greus A., Ek M., Karlsson S.: Water absorption and hydrothermal performance of PHBV/sisal biocomposites. Polymer Degradation and Stability, **108**, 166–174 (2014). https://doi.org/10.1016/j.polymdegradstab.2014.04.012

[2] Arcos-Hernández M. V., Laycock B., Donose B. C., Pratt S., Halley P., Al-Luaibi S., Werker A., Lant P. A.: Physicochemical and mechanical properties of mixed culture polyhydroxyalkanoate (PHBV). European Polymer Journal, **49**, 904–913 (2013). https://doi.org/10.1016/j.eurpolymj.2012.10.025

[3] Ulery B. D., Nair L. S., Laurencin C. T.: Biomedical applications of biodegradable polymers. Journal of Polymer Science Part B: Polymer Physics, **49**, 832–864 (2011). https://doi.org/10.1002/polb.22259

[4] Wang Y., Lu L., Zheng Y., Chen X.: Improvement in hydrophilicity of PHBV films by plasma treatment. Journal of Biomedical Materials Research Part A, **76**, 589–595 (2006). https://doi.org/10.1002/jbm.a.30575

[5] Avella M., Martuscelli E., Raimo M.: Properties of blends and composites based on poly(3-hydroxy)butyrate (PHB) and poly(3-hydroxybutyrate-hydroxyvalerate) (PHBV) copolymers. Journal of Materials Science, **35**, 523–545 (2000). https://doi.org/10.1023/A:1004740522751

[6] Anžlovar A., Kržan A., Žagar E.: Degradation of PLA/ZnO and PHBV/ZnO composites prepared by melt processing. Arabian Journal of Chemistry, **11**, 343–352 (2018). https://doi.org/10.1016/j.arabjc.2017.07.001

[7] Gonçalves S. P. C., Martins-Franchetti S. M.: Action of soil microorganisms on PCL and PHBV blend and films. Journal of Polymers and the Environment, **18**, 714–719 (2010). https://doi.org/10.1007/s10924-010-0209-9

[8] Rutkowska M., Krasowska K., Heimowska A., Adamus G., Sobota M., Musioł M., Janeczek H., Sikorska W., Krzan A., Žagar E., Kowalczuk M.: Environmental degradation of blends of atactic poly[(R,S)-3-hydroxybutyrate] with natural PHBV in Baltic Sea water and compost with activated sludge. Journal of Polymers and the Environment, **16**, 183–191 (2008). https://doi.org/10.1007/s10924-008-0100-0

[9] Gonçalves S. P. C., Martins-Franchetti S. M., Chinaglia D. L.: Biodegradation of the films of PP, PHBV and its blend in soil. Journal of Polymers and the Environment, **17**, 280–285 (2009). https://doi.org/10.1007/s10924-009-0150-y

[10] Batista K. C., Silva D. A. K., Coelho L. A. F., Pezzin S. H., Pezzin A. P. T.: Soil biodegradation of PHBV/peach palm particles biocomposites. Journal of Polymers and the Environment, **18**, 346–354 (2010). https://doi.org/10.1007/s10924-010-0238-4

[11] Arcos-Hernandez M. V., Laycock B., Pratt S., Donose B. C., Nikolić M. A. L., Luckman P., Werker A., Lant P. A.: Biodegradation in a soil environment of activated sludge derived polyhydroxyalkanoate (PHBV). Polymer Degradation and Stability, **97**, 2301–2312 (2012). https://doi.org/10.1016/j.polymdegradstab.2012.07.035

[12] Weng Y-X., Wang Y., Wang X-L., Wang Y-Z.: Biodegradation behavior of PHBV films in a pilot-scale composting condition. Polymer Testing, **29**, 579–587 (2010). https://doi.org/10.1016/j.polymertesting.2010.04.002

[13] Salomez M., George M., Fabre P., Touchaleaume F., Cesar G., Lajarrige A., Gastaldi E.: A comparative study of degradation mechanisms of PHBV and PBSA under laboratory-scale composting conditions. Polymer Degradation and Stability, **167**, 102–113 (2019). https://doi.org/10.1016/j.polymdegradstab.2019.06.025

[14] Shah A. A., Hasan F., Hameed A., Ahmed S.: Isolation and characterisation of poly(3-hydroxybutyrate-*co*-3-hydroxyvalerate) degrading actinomycetes and purification of PHBV depolymerase from newly isolated-Streptoverticillium kashmirense AF1. Annals of Microbiology, **57**, 583–588 (2007). https://doi.org/10.1007/BF03175359

[15] Kang I-K., Kim J. C.: Electrospun composite nanofibrous scaffolds for tissue engineering. in 'Biomaterials in Asia' (ed.: Tateishi T.) 194–206 (2008). https://doi.org/10.1142/9789812835758_0012

[16] Li Z., Lin H., Ishii N., Chen G-Q., Inoue Y.: Study of enzymatic degradation of microbial copolyesters consisting of 3-hydroxybutyrate and medium-chain-length 3-hydroxyalkanoates. Polymer Degradation and Stability, **92**, 1708–1714 (2007). https://doi.org/10.1016/j.polymdegradstab.2007.06.001

[17] Liu Q-S., Zhu M-F., Wu W-H., Qin Z-Y.: Reducing the formation of six-membered ring ester during thermal degradation of biodegradable PHBV to enhance its thermal stability. Polymer Degradation and Stability, **94**, 18–24 (2009). https://doi.org/10.1016/j.polymdegradstab.2008.10.016

[18] Wei L., McDonald A. G.: Accelerated weathering studies on the bioplastic, poly(3-hydroxybutyrate-*co*-3-hydroxyvalerate). Polymer Degradation and Stability, **126**, 93–100 (2016). https://doi.org/10.1016/j.polymdegradstab.2016.01.023

[19] Antunes A., Popelka A., Aljarod O., Hassan M. K., Kasak P., Luyt A. S.: Accelerated weathering effects on poly(3-hydroxybutyrate-*co*-3-hydroxyvalerate) (PHBV) and PHBV/TiO_2 nanocomposites. Polymers, **12**, 1–28 (2020). https://doi.org/10.3390/POLYM12081743

[20] Feng P., Jia J., Liu M., Peng S., Zhao Z., Shuai C.: Degradation mechanisms and acceleration strategies of poly (lactic acid) scaffold for bone regeneration. Materials and Design, **210**, 110066 (2021). https://doi.org/10.1016/j.matdes.2021.110066

[21] Shuai C., Yang W., Feng P., Peng S., Pan H.: Accelerated degradation of HAP/PLLA bone scaffold by PGA blending facilitates bioactivity and osteoconductivity. Bioactive Materials, **6**, 490–502 (2021). https://doi.org/10.1016/j.bioactmat.2020.09.001

[22] Abdulkareem A., Kasak P., Nassr M. G., Mahmoud A. A., Al-Ruweidi M. K. A. A., Mohamoud K. J., Hussein M. K., Popelka A.: Surface modification of poly(lactic acid) film *via* cold plasma assisted grafting of fumaric and ascorbic acid. Polymers, **2021**, 3717 (2021). https://doi.org/10.3390/POLYM13213717

[23] Jelil R. A.: A review of low-temperature plasma treatment of textile materials. Journal of Materials Science, **50**, 5913–5943 (2015). https://doi.org/10.1007/S10853-015-9152-4

[24] Morent R., De Geyter N., Desmet T., Dubruel P., Leys C.: Plasma surface modification of biodegradable polymers: A review. Plasma Processes and Polymers, **8**, 171–190 (2011). https://doi.org/10.1002/PPAP.201000153

[25] Rudolph A., Teske M., Illner S., Kiefel V., Sternberg K., Grabow N., Wree A., Hovakimyan M.: Surface modification of biodegradable polymers towards better biocompatibility and lower thrombogenicity. PLoS ONE, **10**, 142075 (2015). https://doi.org/10.1371/JOURNAL.PONE.0142075

[26] De Geyter N., Morent R.: Cold plasma surface modification of biodegradable polymer biomaterials. in 'Biomaterials for Bone Regeneration: Novel Techniques and Applications' (eds.: Dubruel P., van Vlierberghe S.) Elsevier, Amsterdam 202–224 (2014). https://doi.org/10.1533/9780857098104.2.202

[27] Ferreira B. M. P., Pinheiro L. M. P., Nascente P. A. P., Ferreira M. J., Duek E. A. R.: Plasma surface treatments of poly(L-lactic acid) (PLLA) and poly(hydroxybutyrate-*co*-hydroxyvalerate) (PHBV). Materials Science and Engineering C, **29**, 806–813 (2009). https://doi.org/10.1016/j.msec.2008.07.026

[28] Chang S-H., Chian C-H.: Plasma surface modification effects on biodegradability and protein adsorption properties of chitosan films. Applied Surface Science, **282**, 735–740 (2013). https://doi.org/10.1016/j.apsusc.2013.06.044

[29] Fabbri M., Gigli M., Costa M., Govoni M., Seri P., Lotti N., Giordano E., Munari A., Gamberini R., Rimini B., Neretti G., Cristofolini A., Borghi C. A.: The effect of plasma surface modification on the biodegradation rate and biocompatibility of a poly(butylene succinate)-based copolymer. Polymer Degradation and Stability, **121**, 271–279 (2015). https://doi.org/10.1016/j.polymdegradstab.2015.09.015

[30] Hasirci V., Tezcaner A., Hasirci N., Süzer Ş.: Oxygen plasma modification of poly(3-hydroxybutyrate-*co*-3-hydroxyvalerate) film surfaces for tissue engineering purposes. Journal of Applied Polymer Science, **87**, 1285–1289 (2002). https://doi.org/10.1002/app.11532

[31] Mirmohammadi S. A., Khorasani M. T., Mirzadeh H., Irani S.: Investigation of plasma treatment on poly(3-hydroxybutyrate) film surface: Characterization and *in vitro* assay. Polymer-Plastics Technology and Engineering, **51**, 1319–1326 (2012). https://doi.org/10.1080/03602559.2012.701365

[32] Kim M. C., Masuoka T.: Degradation properties of PLA and PHBV films treated with CO_2-plasma. Reactive and Functional Polymers, **69**, 287–292 (2009). https://doi.org/10.1016/j.reactfunctpolym.2009.01.013

[33] Denes F. S., Manolache S.: Macromolecular plasma-chemistry: An emerging field of polymer science. Progress in Polymer Science, **29**, 815–885 (2004). https://doi.org/10.1016/j.progpolymsci.2004.05.001

[34] Owens D. K., Wendt R. C.: Estimation of the surface free energy of polymers. Journal of Applied Polymer Science, **13**, 1741–1747 (1969). https://doi.org/10.1002/app.1969.070130815

[35] Scandola M., Ceccorulli G., Pizzoli M., Gazzano M.: Study of the crystal phase and crystallization rate of bacterial poly(3-hydroxybutyrate-*co*-3-hydroxyvalerate). Macromolecules, **25**, 1405–1410 (1992). https://doi.org/10.1021/ma00031a008

[36] Wang Y., Lu L., Zheng Y., Chen X.: Improvement in hydrophilicity of PHBV films by plasma treatment. Journal of Biomedical Materials Research, **76A**, 589–595 (2005). https://doi.org/10.1002/jbm.a.30575

[37] Tverdokhlebov S. I., Bolbasov E. N., Shesterikov E. V., Antonova L. V., Golovkin A. S., Matveeva V. G., Petlin D. G., Anissimov Y. G.: Modification of polylactic acid surface using RF plasma discharge with sputter deposition of a hydroxyapatite target for increased biocompatibility. Applied Surface Science, **329**, 32–39 (2015). https://doi.org/10.1016/j.apsusc.2014.12.127

[38] Ubaid F., Radwan A. B., Naeem N., Shakoor R. A., Ahmad Z., Montemor M. F., Kahraman R., Abdullah A. M., Soliman A.: Multifunctional self-healing polymeric nanocomposite coatings for corrosion inhibition of steel. Surface and Coatings Technology, **372**, 121–133 (2019). https://doi.org/10.1016/j.surfcoat.2019.05.017

[39] Yang Z., Peng H., Wang W., Liu T.: Crystallization behavior of poly(ε-caprolactone)/layered double hydroxide nanocomposites. Journal of Applied Polymer Science, **116**, 2658–2667 (2010). https://doi.org/10.1002/app.31787

[40] do Nascimento Silva R., da Silva L. R. C., de Morais A. C. L., Alves T. S., Barbosa R.: Study of the hydrolytic degradation of poly-3-hydroxybutyrate in the development of blends and polymeric bionanocomposites. Journal of Thermoplastic Composite Materials, **34**, 884–901 (2021). https://doi.org/10.1177/0892705719856044

[41] Antunes A., Popelka A., Aljarod O., Hassan M. K., Luyt A. S.: Effects of rutile–TiO_2 nanoparticles on accelerated weathering degradation of poly(lactic acid). Polymers, **12**, 1096 (2020). https://doi.org/10.3390/polym12051096

[42] Kaynak C., Sari B.: Accelerated weathering performance of polylactide and its montmorillonite nanocomposite. Applied Clay Science, **121–122**, 86–94 (2016). https://doi.org/10.1016/j.clay.2015.12.025

[43] Lv S., Liu X., Gu J., Jiang Y., Tan H., Zhang Y.: Effect of glycerol introduced into PLA based composites on the UV weathering behavior. Construction and Building Materials, **144**, 525–531 (2017). https://doi.org/10.1016/j.conbuildmat.2017.03.209

[44] Luo Y., Cao Y., Guo G.: Effects of TiO_2 nanoparticles on the photodegradation of poly(lactic acid). Journal of Applied Polymer Science, **135**, 46509 (2018). https://doi.org/10.1002/app.46509

[45] Cintrón M. S., Hinchliffe D. J.: FT-IR examination of the development of secondary cell wall in cotton fibers. Fibers, **3**, 30–40 (2015). https://doi.org/10.3390/fib3010030

[46] Slepička P., Kasálková N. S., Stránská E., Bačáková L., Švorčík V.: Surface characterization of plasma treated polymers for applications as biocompatible carriers. Express Polymer Letters, **7**, 535–545 (2013). https://doi.org/10.3144/expresspolymlett.2013.50

[47] Vesel A., Primc G., Zaplotnik R., Mozetič M.: Applications of highly non-equilibrium low-pressure oxygen plasma for treatment of polymers and polymer composites on an industrial scale. Plasma Physics and Controlled Fusion, **62**, 024008 (2020). https://doi.org/10.1088/1361-6587/ab5b50

[48] Cools P., de Geyter N., Morent R.: PLA enhanced *via* plasma technology: A review. in 'New developments in polylactic acid research' (ed.: Winthrop C.) Nova Science, New York, 79–110 (2015).

[49] Nabedryk E., Breton J.: Polarized Fourier transform infrared (FTIR) difference spectroscopy of the M412 intermediate in the bacteriorhodopsin photocycle. FEBS Letters, **202**, 356–360 (1986). https://doi.org/10.1016/0014-5793(86)80718-9

[50] Buzarovska A., Grozdanov A.: Crystallization kinetics of poly(hydroxybutyrate-*co*-hydroxyvalerate) and poly (dicyclohexylitaconate) PHBV/PDCHI blends: Thermal properties and hydrolytic degradation. Journal of Materials Science, **44**, 1844–1850 (2009). https://doi.org/10.1007/s10853-008-3236-3

[51] Varsavas S. D., Kaynak C.: Weathering degradation performance of PLA and its glass fiber reinforced composite. Materials Today Communications, **15**, 344–353 (2018). https://doi.org/10.1016/j.mtcomm.2017.11.008

[52] Sadi R. K., Fechine G. J. M., Demarquette N. R.: Photodegradation of poly(3-hydroxybutyrate). Polymer Degradation and Stability, **95**, 2318–2327 (2010). https://doi.org/10.1016/j.polymdegradstab.2010.09.003

[53] Martinez-Colunga J. G., Sanchez-Valdes S., Ramos-de-Valle L. F., Ramirez-Vargas E., Avila-Orta C., Rodriguez-Gonzalez J. A., Espinoza-González C. J., Benavides-Cantú R., Lozano-Ramírez T.: Effect of ultrasonic irradiation on low-density polyethylene molecular structure. Polymer Bulletin, **77**, 5303–5321 (2020). https://doi.org/10.1007/s00289-019-03006-4

[54] Yang J., Bei J., Wang S.: Enhanced cell affinity of poly (D,L-lactide) by combining plasma treatment with collagen anchorage. Biomaterials, **23**, 2607–2614 (2002). https://doi.org/10.1016/S0142-9612(01)00400-8

[55] Cassie A. B. D., Baxter S.: Wettability of porous surfaces. Transactions of the Faraday Society, **40**, 546–551 (1944). https://doi.org/10.1039/tf9444000546

[56] Iggui K., Kaci M., Le Moigne N., Bergeret A.: The effects of accelerated photooxidation on molecular weight and thermal and mechanical properties of PHBV/cloisite 30B bionanocomposites. Journal of Renewable Materials, **6**, 288–298 (2018). https://doi.org/10.7569/JRM.2017.634184

[57] Rydz J., Wolna-Stypka K., Musioł M., Szeluga U., Janeczek H., Kowalczuk M.: Further evidence of polylactide degradation in paraffin and in selected protic media. A thermal analysis of eroded polylactide films. Polymer Degradation and Stability, **98**, 1450–1457 (2013). https://doi.org/10.1016/j.polymdegradstab.2013.05.005

[58] Panaitescu D. M., Ionita E. R., Nicolae C-A., Gabor A. R., Ionita M. D., Trusca R., Lixandru B-E., Codita I., Dinescu G.: Poly(3-hydroxybutyrate) modified by nanocellulose and plasma treatment for packaging applications. Polymers, **10**, 1–24 (2018). https://doi.org/10.3390/polym10111249

[59] Slepička P., Malá Z., Rimpelová S., Slepičková Kasálková N., Švorčík V.: Plasma treatment of the surface of poly(hydroxybutyrate) foil and non-woven fabric and assessment of the biological properties. Reactive and Functional Polymers, **95**, 71–79 (2015). https://doi.org/10.1016/j.reactfunctpolym.2015.08.010

[60] Yoshida S., Hagiwara K., Hasebe T., Hotta A.: Surface modification of polymers by plasma treatments for the enhancement of biocompatibility and controlled drug release. Surface and Coatings Technology, **233**, 99–107 (2013). https://doi.org/10.1016/j.surfcoat.2013.02.042

[61] Du W., Shao H., He Z., Tang C., Liu Y., Shen T., Zhu Y., Lau W-M., Hui D.: Cross-linking poly(lactic acid) film surface by neutral hyperthermal hydrogen molecule bombardment. Journal of Agricultural and Food Chemistry, **63**, 10604–10610 (2015). https://doi.org/10.1021/acs.jafc.5b04249

[62] Montagna L. S., do Amaral Montanheiro T. L., Passador F. R., Lemes A. P., Rezende M. C.: The influence of artificial photodegradation on properties of poly(3-hydroxybutyrate-*co*-3-hydroxyvalerate)(PHBV)/graphite nanosheets (GNS) nanocomposites. Journal of Polymers and the Environment, **26**, 1511–1519 (2018). https://doi.org/10.1007/s10924-017-1051-0